Entanglement-assisted tomography of a quantum target

A De Pasquale[1]**, P Facchi**[2,3]**, V Giovannetti**[1] **and K Yuasa**[4]

[1] NEST, Scuola Normale Superiore and Istituto Nanoscienze-CNR, I-56126 Pisa, Italy
[2] Dipartimento di Matematica and MECENAS, Università di Bari, I-70125 Bari, Italy
[3] INFN, Sezione di Bari, I-70126 Bari, Italy
[4] Waseda Institute for Advanced Study, Waseda University, Tokyo 169-8050, Japan

E-mail: antonella.depasquale@sns.it

Abstract

We study the efficiency of quantum tomographic reconstruction where the system under investigation (quantum target) is indirectly monitored by looking at the state of a quantum probe that has been scattered off the target. In particular, we focus on the state tomography of a qubit through a one-dimensional scattering of a probe qubit, with a Heisenberg-type interaction. Via direct evaluation of the associated quantum Cramér–Rao bounds, we compare the accuracy efficiency that one can obtain by adopting entanglement-assisted strategies with that achievable when entanglement resources are not available. Even though sub-shot noise accuracy levels are not attainable, we show that quantum correlations play a significant role in the estimation. A comparison with the accuracy levels obtainable by direct estimation (not through a probe) of the quantum target is also performed.

PACS numbers: 03.65.Wj, 03.65.Nk, 06.20.Dk, 72.10.−d

(Some figures may appear in colour only in the online journal)

1. Introduction

The possibility of reconstructing the quantum state of a system via measurements (quantum state tomography (QST)) is a central problem in quantum information theory [1], which poses a series of fundamental questions related to the fact that the state itself is not directly observable and that each given quantum measurement typically reveals only partial information on the observed system. In recent years, a great deal of work has been devoted to this issue and many important features have been recognized, including the fact that having at disposal several copies (say M) of the initial state, collective measurements are more informative than individual ones, e.g., see [1–3] and references therein. In abstract terms, QST ultimately reduces

to the ability of estimating the set of continuous parameters, which define the expansion of an unknown state with respect to a reference basis of operators (say the set of Pauli's matrices for a two-level system, qubit). As such, its ultimate accuracy limits can be evaluated by exploiting some general results of quantum estimation theory [4, 5, 9, 10] (more precisely, of a part of the theory which directly deals with the estimation of continuous parameters).

Up to now, most of the works focused on scenarios where the system under investigation can be directly accessed, i.e. posing no constraint whatsoever to the physical operations one may perform on it. In this context, for instance, the ultimate accuracy limit obtainable in the tomographic reconstruction of a qubit initialized in an arbitrary (possibly) mixed state has been set in [3], by computing the associated quantum Cramér–Rao (CR) bound [4, 5, 22], in terms of the quantum Fisher information (QFI) matrix of the problem (see below for the precise definitions). In this paper, instead, we address the problem from a slightly different perspective, which captures an important aspect of many realistic experimental situations. More precisely, along the line set in [11], we consider the case in which the system of interest (from now on the *target X*) can only be addressed indirectly via measurements performed on a probe which has interacted with it. In our model, the latter is described as a quantum system A characterized both by external (e.g., momentum/position) and internal (e.g., spin) degrees of freedom, which the experimentalists are allowed to prepare in any initial configuration (also the target possesses external *and* internal degrees of freedoms but, for the sake of simplicity, only the latter are supposed to be unknown, the external degrees of freedom being assigned by fixing the position of the target system). The tomographic reconstruction then proceeds by letting that A and X interact via a scattering process and by measuring the final state of the former (or at least a part of it which has been scattered along some preferred direction). Indeed, the whole setting is devised in order to mimic the basic features of a standard (Rutherford-like) scattering experiment, where one tries to reconstruct the properties of a target system by firing probe particles on it and by looking at the way they emerge from the process. For the sake of simplicity, we will limit the analysis to the case of 1D scattering processes and describe the internal degrees of freedom of A and X as two-level (spin) systems (similar models have been recently analyzed to study entanglement generation [12, 13]).

It is worth noting that the problem we are considering admits also an interpretation in the context of *quantum channel estimation* theory (see [10] and references therein). This is the theory, sometimes identified with the name of *quantum metrology*, which studies the efficiency of those schemes designed to recover information not on a quantum system, but on a quantum channel (quantum process tomography (QPT)). We recall that in quantum mechanics quantum channels represent the most general physical transformations and are fully described by assigning completely positive trace-preserving linear (CPTL) mappings [5], which act on the density matrices of the system (in our case the probe A). In quantum metrology, the mapping Φ_v is assumed to belong to a family of transformations identified by a set of parameters v, whose values are unknown and which we wish to recover by preparing the system in some fiduciary initial state ρ_A^{in} and by measuring the corresponding output state transformed by the channel. In our case, the quantum channel to be estimated is the one that induces a modification on the probe A via its interaction with the target X, while the v's correspond to the parameters that define the (unknown) state ρ_X (see figure 1). In the jargon introduced in [15], this transformation belongs to the special class of *programmable channels*[5].

---

[5] Explicitly, these channels can indeed be parametrized by assigning a fixed interaction with an external unknown system. In a seminal paper [6], Nielsen and Chuang proved that the family of all unitaries acting on n qubits is not programmable, since an n-qubit register can encode at most 2^n distinct quantum operations. Notwithstanding the non-universality of programmable channels, the authors also pointed out the possibility of programming the family
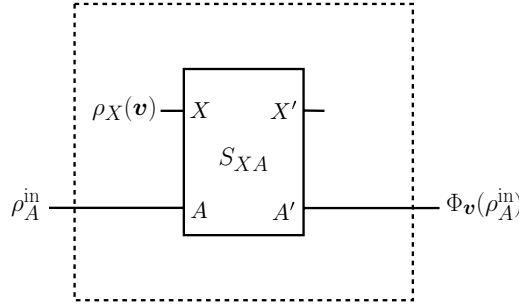
Figure 1. Scheme of a programmable quantum channel. Here, the CPTL map $\Phi_{\boldsymbol{v}}$ is defined as an interaction with an external system X through a given (fixed) coupling represented by the operator S_{XA}. In our problem, the channel to be reconstructed describes the 1D scattering of a probe A off a target qubit X, with the Heisenberg-type interaction. This process induces a modification of the probe initial state ρ_A^{in} according to the target initial state $\rho_X(\boldsymbol{v})$ identified by the coordinates $\boldsymbol{v}$.

A well-known fact is that, in general, if M is the number of tests we perform in order to recover the actual values of $\boldsymbol{v}$ (each test consisting of applying the *same* channel $\Phi_{\boldsymbol{v}}$ to a new copy of probe A), the statistical scaling of the associated uncertainty can be reduced from the 'standard quantum limit' (SQL) (or 'shot noise' in quantum optics) $1/\sqrt{M}$ scaling, to the so-called 'Heisenberg bound' $1/M$ scaling, by the introduction of suitable quantum correlations between initializations of the various copies of A [10, 14]. However, this is not the case if, as in our case, the channels under investigation are programmable [15]. As a consequence, in our model, no sub-shot noise scaling in M of the accuracy should be expected. For this reason, we will limit the analysis to those configurations in which the M tests on X are performed by preparing M copies of A in the same initial state. The QFI matrix approach [4, 5, 9] will then be used to evaluate the associated accuracy, optimizing it with respect to the initial preparation of A (with respect to both its internal and external degrees of freedom) and comparing it with the results obtained in [3] for the case of direct estimation. Most importantly, we will also study an entanglement-assisted (EA) strategy, where each copy of A is initialized into an entangled state of A with an external ancilla system B, which does not interact directly with X (see figure 2), showing a clear improvement in the performance of the estimation process with respect to the non-EA (NEA) strategy in line with the findings of [14, 16].

This paper is organized as follows. In section 2, we introduce our scattering model and briefly review some basic aspects of quantum estimation theory. Then, in sections 3 and 4, we will discuss two different strategies for the tomographic reconstruction of the target qubit, with and without the help of quantum correlations in the probe preparation. In particular, in section 3, we first derive the exact expression for the QFI matrix in the case of an EA configuration, in which the probe is initialized in a maximally entangled state with the ancilla system, and discuss some applications of the result in the evaluation of some functionals of the state of the target (specifically its purity and its azimuthal angle). In section 4, instead, we compare the EA and NEA cases by focusing on a special configuration in which the target state is characterized by a single unknown parameter. The paper ends with section 5 by summarizing our results in the light of future perspectives. The more technical aspects of the derivation are presented in a couple of appendices.

of unitary operations probabilistically. In this context, an interesting model was proposed for the case of single qubits in [7] and implemented for photonic qubits in [8].
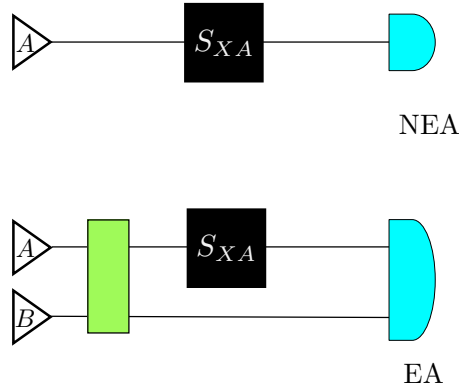
Figure 2. Strategies for the estimation of the target parameters. In the NEA strategy, the probe *A* and the ancilla system *B* are in a separable state and, as will be clarified in section 4, this analysis can be performed by completely neglecting *B*. On the other hand, in the EA strategy quantum correlations are introduced (rectangular box). In both schemes, one makes use of optimal POVMs for the estimation of the target parameters. Note that only qubit *A* undergoes a direct interaction (S_{XA}) with the target *X*.

2. The model

In this section, we introduce the model and set up the notation.

2.1. 1D scattering of the probe A

Suppose that a target qubit *X* is fixed at a given position $x = 0$ on a line and that its unknown state is described by the density matrix

$$\rho_X(\boldsymbol{v}) = \frac{1 + \boldsymbol{v} \cdot \boldsymbol{\sigma}_X}{2}, \qquad 0 \leqslant |\boldsymbol{v}| \leqslant 1, \tag{1}$$

with $\boldsymbol{\sigma} = (\sigma^x, \sigma^y, \sigma^z)$ being the Pauli operators and $\boldsymbol{v} = (v_x, v_y, v_z)$ the 3D Bloch vector, which represents the set of parameters we wish to recover via QST. In [11], it was shown that $\boldsymbol{v}$ (and hence $\rho_X(\boldsymbol{v})$) can be obtained from the transmission and reflection probabilities of a probe qubit *A* scattered off *X* through a point-like interaction, which couples the internal degrees of freedom of the two qubits via the following Heisenberg-type Hamiltonian:

$$H = \frac{p_A^2}{2m} + g(\boldsymbol{\sigma}_X \cdot \boldsymbol{\sigma}_A)\delta(x_A). \tag{2}$$

Here, *m* and p_A are the mass and the momentum operators of *A*, *g* is a positive coupling constant and $\boldsymbol{\sigma}_J$ are the Pauli operators acting on the qubit *J* (= *X*, *A*). Specifically, in [11], *A* was assumed to be initialized into a known input state $|k\rangle\langle k| \otimes \rho_A^{\text{in}}$ and injected from the left of the line with momentum $\hbar k > 0$. This kind of systems can be considered as models for a magnetic impurity spin embedded along a 1D wire [17], such as a semiconductor quantum wire [18] or a single-wall carbon nanotube [19]. For instance, an electron is sent through the 1D wire as a probe particle, and its spin state is resolved after the scattering by spin-sensitive filters [20]. Alternatively, an electron populating the lowest sub-band of the 1D wire can undergo scattering from two double quantum dots [21] to which it is electrostatically coupled. The state tomography of $\rho_X(\boldsymbol{v})$ then proceeded by solving the associated scattering problem and looking at the state of *A* which emerges either on the left (transmitted component) or on

the right (reflected component), or both. Such states admit a simple expression in terms of the scattering matrix S_{XA} of the process defined by the unitary operator:

$$S_{XA} = \int dk\, |k\rangle\langle k| \otimes S^t_{XA} + \int dk\, |-k\rangle\langle k| \otimes S^r_{XA}, \tag{3}$$

with

$$S^{t\dagger}_{XA} S^t_{XA} + S^{r\dagger}_{XA} S^r_{XA} = 1, \qquad S^{t\dagger}_{XA} S^r_{XA} + S^{r\dagger}_{XA} S^t_{XA} = 0. \tag{4}$$

Here, the $|k\rangle$'s represent the momentum eigenstates of the probe A ($\hbar k$ being the associated eigenvalues), while the 4×4 matrices S^t_{XA} and S^r_{XA} define the spin-dependent scattering amplitudes associated with transmission and reflection events, respectively. They are functions of the probe wave number k and are given by

$$S^{t,r}_{XA} = \alpha_{t,r}(\Omega) + \beta_{t,r}(\Omega)(\boldsymbol{\sigma}_X \cdot \boldsymbol{\sigma}_A), \tag{5}$$

with Ω being the dimensionless parameter:

$$\Omega = \frac{mg}{\hbar|k|}, \tag{6}$$

and

$$\alpha_t(\Omega) = \frac{1 - 2i\Omega}{(1 - 3i\Omega)(1 + i\Omega)}, \qquad \beta_t(\Omega) = \frac{-i\Omega}{(1 - 3i\Omega)(1 + i\Omega)}, \tag{7}$$

$$\alpha_r(\Omega) = \frac{-3\Omega^2}{(1 - 3i\Omega)(1 + i\Omega)}, \qquad \beta_r(\Omega) = \beta_t(\Omega). \tag{8}$$

For an explicit derivation of all these equations, we refer the reader to [11].

Consider now an experimental setting in which an observer tries to reconstruct $\rho_X(\boldsymbol{v})$ by merging incoherently[6] the data associated with the transmission events (to the right of the target) and the reflection events (to the left). The final state of A can be expressed as the tensor product of effective *qutrit* density operators

$$\rho^{t+r}_A(\boldsymbol{v}) = |e^r\rangle_A\langle e^r| \otimes \mathrm{Tr}_X \left\{ S^t_{XA} [\rho_X(\boldsymbol{v}) \otimes \rho^{\mathrm{in}}_A] S^{t\dagger}_{XA} \right\}$$
$$+ \mathrm{Tr}_X \left\{ S^r_{XA} [\rho_X(\boldsymbol{v}) \otimes \rho^{\mathrm{in}}_A] S^{r\dagger}_{XA} \right\} \otimes |e^t\rangle_A\langle e^t|, \tag{9}$$

where $\mathrm{Tr}_X\{\cdots\}$ is the partial trace over X, and $|e^t\rangle_A$ ($|e^r\rangle_A$) is a vector orthogonal to *all* the internal spin states of A, which represents the *vacuum state* associated with no particle reaching the rhs (lhs) detector. The first term represents the contribution associated with a transmitted A reaching the rhs detector (vacuum on the lhs), while the second represents the opposite one (i.e. spin on the lhs and vacuum on the rhs). The detectors are assumed to have 100% efficiency and no particle creation or destruction by the target is possible so that the number of particles is conserved: every incident particle emerges *either* from the left *or* from the right of the target.

On the other hand, if the observer collects only transmitted particles, emerging from the rhs of the target, he/she will either see nothing (A being reflected by X) or see A emerging with the same momentum $\hbar k$ it had when entering the line but with a modified spin state due to the interaction with X. Such configuration is described by the density operator, obtained from $\rho^{t+r}_A(\boldsymbol{v})$ by tracing out the reflected case, namely

$$\rho^t_A(\boldsymbol{v}) = \mathrm{Tr}_r \rho^{t+r}_A(\boldsymbol{v})$$
$$= \mathrm{Tr}_X \left\{ S^t_{XA} [\rho_X(\boldsymbol{v}) \otimes \rho^{\mathrm{in}}_A] S^{t\dagger}_{XA} \right\} + \mathrm{Tr} \left\{ S^r_{XA} [\rho_X(\boldsymbol{v}) \otimes \rho^{\mathrm{in}}_A] S^{r\dagger}_{XA} \right\} |e^t\rangle_A\langle e^t|. \tag{10}$$

---

[6] By incoherent merging of the transmitted and reflected data, we mean that no joint measurements are allowed on the transmitted and reflected signals (a scenario which is realistic if the rhs and lhs detectors are located sufficiently apart from each other).

Note that here

$$\text{Tr}\left\{S_{XA}^r\big[\rho_X(\boldsymbol{v})\otimes\rho_A^{\text{in}}\big]S_{XA}^{r\dagger}\right\}=1-\text{Tr}\{S_{XA}^t[\rho_X(\boldsymbol{v})\otimes\rho_A^{\text{in}}]S_{XA}^{t\dagger}\} \tag{11}$$

is the reflection probability (i.e. the probability of no detection of A on the rhs of the line).

An analogous expression holds for the alternative experimental setting in which the observer only collects information of the signals emerging from the lhs of the line. In this case, equation (10) is replaced by

$$\begin{aligned}
\rho_A^r(\boldsymbol{v}) &= \text{Tr}_t\,\rho_A^{t+r}(\boldsymbol{v}) \\
&= \text{Tr}\left\{S_{XA}^t\big[\rho_X(\boldsymbol{v})\otimes\rho_A^{\text{in}}\big]S_{XA}^{t\dagger}\right\}|e^r\rangle_A\langle e^r|+\text{Tr}_X\left\{S_{XA}^r\big[\rho_X(\boldsymbol{v})\otimes\rho_A^{\text{in}}\big]S_{XA}^{r\dagger}\right\}.
\end{aligned} \tag{12}$$

The output density matrices $\rho_A^{t+r/t/r}(\boldsymbol{v})$, associated with the three different experimental settings, are the functions of the state $\rho_X(\boldsymbol{v})$ of X. Therefore, one can acquire information on the latter by performing QST on the former. Furthermore, since $\rho_A^{t+r/t/r}(\boldsymbol{v})$ also depends on the input state ρ_A^{in} and on the input momentum $\hbar k$ of the probe A, one can try to optimize the resulting accuracy with respect to these parameters.

2.2. EA scheme

An interesting variation of the previous schemes is obtained by considering the case in which A is prepared into a joint (possibly entangled) state ρ_{AB}^{in} with an ancilla system B, which is not directly interacting with X (see figure 2). Such EA configurations proved to be successful in boosting the efficiency of several quantum estimation [16] and discrimination schemes [23].

Assuming that B sits at rest in the laboratory of the observer, the resulting states of AB emerging from the AX interaction can again be expressed in terms of the scattering matrix S_{XA} given before. Specifically, equations (9), (10) and (12) become

$$\begin{aligned}
\rho_{AB}^{t+r}(\boldsymbol{v}) &= |e^r\rangle_A\langle e^r|\otimes\text{Tr}_X\{(S_{XA}^t\otimes\mathbb{I}_B)[\rho_X(\boldsymbol{v})\otimes\rho_{AB}^{\text{in}}](S_{XA}^{t\dagger}\otimes\mathbb{I}_B)\} \\
&\quad+\text{Tr}_X\{(S_{XA}^r\otimes\mathbb{I}_B)[\rho_X(\boldsymbol{v})\otimes\rho_{AB}^{\text{in}}](S_{XA}^{r\dagger}\otimes\mathbb{I}_B)\}\otimes|e^t\rangle_A\langle e^t|,
\end{aligned} \tag{13}$$

$$\begin{aligned}
\rho_{AB}^t(\boldsymbol{v}) &= \text{Tr}_r\,\rho_{AB}^{t+r} \\
&= \text{Tr}_X\{(S_{XA}^t\otimes\mathbb{I}_B)[\rho_X(\boldsymbol{v})\otimes\rho_{AB}^{\text{in}}](S_{XA}^{t\dagger}\otimes\mathbb{I}_B)\} \\
&\quad+\text{Tr}_{XA}\{(S_{XA}^r\otimes\mathbb{I}_B)[\rho_X(\boldsymbol{v})\otimes\rho_{AB}^{\text{in}}](S_{XA}^{r\dagger}\otimes\mathbb{I}_B)\}\otimes|e^t\rangle_A\langle e^t|,
\end{aligned} \tag{14}$$

$$\begin{aligned}
\rho_{AB}^r(\boldsymbol{v}) &= \text{Tr}_t\,\rho_{AB}^{t+r} \\
&= |e^r\rangle_A\langle e^r|\otimes\text{Tr}_{XA}\{(S_{XA}^t\otimes\mathbb{I}_B)[\rho_X(\boldsymbol{v})\otimes\rho_{AB}^{\text{in}}](S_{XA}^{t\dagger}\otimes\mathbb{I}_B)\} \\
&\quad+\text{Tr}_X\{(S_{XA}^r\otimes\mathbb{I}_B)[\rho_X(\boldsymbol{v})\otimes\rho_{AB}^{\text{in}}](S_{XA}^{r\dagger}\otimes\mathbb{I}_B]\},
\end{aligned} \tag{15}$$

where $\mathbb{I}_B$ stands for the identity operator on B.

2.3. The Cramér–Rao bound

In the following sections, we will compare the accuracy one can obtain by reconstructing $\rho_X(\boldsymbol{v})$ through the EA configurations via measurements on the output states $\rho_{AB}^{t+r/t/r}(\boldsymbol{v})$ defined by equations (13), (14) and (15), with the corresponding accuracy that one achieves with the NEA configurations associated with the output states $\rho_A^{t+r/t/r}(\boldsymbol{v})$ of equations (9), (10) and (12). Differently from [11] but in line with the approach of [3, 9], such accuracies will be evaluated by computing the corresponding quantum CR bounds [4, 5, 9].

We recall that the quantum CR theorem establishes a fundamental lower bound on the uncertainty of any estimation strategy devised to recover the three components of $\boldsymbol{v}$.

Specifically, assume that one has M copies of the state $\rho(\boldsymbol{v})$, which encodes such parameters. (In our case, for the NEA setting $\rho(\boldsymbol{v})$ is given by the states $\rho_A^{t+r/t/r}(\boldsymbol{v})$, depending on whether the observer collects both transmitted and reflected data, or only transmitted or reflected data. Similarly for the EA setting, where $\rho(\boldsymbol{v})$ is identified with $\rho_{AB}^{t+r/t/r}(\boldsymbol{v})$). A generic estimation strategy consists in assigning a (possibly joint) POVM measurement on the M copies of the state, and a classical data processing scheme that starting from the measurement outcome produces an estimation $\boldsymbol{v}^{\text{est}} = (v_1^{\text{est}}, v_2^{\text{est}}, v_3^{\text{est}})$ of the parameters $\boldsymbol{v}$. The uncertainty of the estimation can then be evaluated by means of the covariance matrix $\text{Cov}[\boldsymbol{v}]_{jk} = \overline{(v_j^{\text{est}} - v_j)(v_k^{\text{est}} - v_k)}$ ($j, k \in \{x, y, z\}$) obtained by averaging the distances between the real value of the parameter $\boldsymbol{v}$ and their estimations. In this context, the CR bound implies that, independently from the adopted POVM and classical data processing scheme, such matrix must verify the inequality [22]

$$\text{Cov}[\boldsymbol{v}] \geqslant \frac{1}{M} \boldsymbol{H}(\boldsymbol{v})^{-1}, \tag{16}$$

where $\boldsymbol{H}(\boldsymbol{v})$ is the QFI matrix of the encoding state [4, 9], i.e.

$$\boldsymbol{H}_{jk} = \sum_n \frac{(\partial_j \rho_n)(\partial_k \rho_n)}{\rho_n} + 2 \,\text{Re} \sum_{n \neq m} \frac{(\rho_n - \rho_m)^2}{\rho_n + \rho_m} \langle \psi_n | \partial_j \psi_m \rangle \langle \partial_k \psi_m | \psi_n \rangle. \tag{17}$$

Here, $\rho(\boldsymbol{v}) = \sum_n \rho_n |\psi_n\rangle\langle\psi_n|$ is the spectral decomposition of the encoding state $\rho(\boldsymbol{v})$, while ∂_j stands for the partial derivative with respect to the jth component v_j of the vector $\boldsymbol{v}$. The jth diagonal element of inequality (16) provides the CR bound for the variance associated with the accuracy in the estimation of the parameter v_j, for fixed values of the others, i.e.[7]

$$\text{Cov}[\boldsymbol{v}]_{jj} = \text{Var}[v_j] = \overline{(v_j^{\text{est}} - v_j)^2} \geqslant \frac{1}{M} (\boldsymbol{H}^{-1})_{jj}. \tag{18}$$

(Note the $1/\sqrt{M}$ SQL scaling of $\sqrt{\text{Var}[v_j]}$.) It is worth observing that even though the bound (16) is not always attainable, the bound (18) is known to be asymptotically achievable for a sufficiently large M. More generally, equation (16) permits also to derive an accuracy bound on the variance of the estimation of any given function $f = f(\boldsymbol{v})$ of the parameters $\boldsymbol{v}$ [4, 9]. Specifically, by re-parameterizing the problem with a new set of independent parameters $\tilde{\boldsymbol{v}} = (\tilde{v}_1(\boldsymbol{v}), \tilde{v}_2(\boldsymbol{v}), \tilde{v}_3(\boldsymbol{v}))$, which include the quantity of interest as (say) the first element $\tilde{v}_1(\boldsymbol{v}) = f(\boldsymbol{v})$, one obtains

$$\text{Var}[f] \geqslant \frac{1}{M} (\tilde{\boldsymbol{H}}^{-1})_{11}, \tag{19}$$

where $\tilde{\boldsymbol{H}} = B H B^T$ is the QFI matrix of the parameters $\tilde{\boldsymbol{v}}$ obtained from $\boldsymbol{H}$ via the similarity transformation induced by the Jacobian matrix $B_{jk} = \partial v_k / \partial \tilde{v}_j$. As in the case of equation (18), for fixed values of $\tilde{v}_2$ and $\tilde{v}_3$, inequality (19) establishes a bound on the accuracy reachable in the estimation of the function f (the bound being achievable for a sufficiently large M under the assumption that $\tilde{v}_2$ and $\tilde{v}_3$ are known *a priori*).

As an application of the above construction, and for future reference, it is instructive to report the quantum CR bounds associated with a direct estimation of $\rho_X(\boldsymbol{v})$, which has been first computed in [3]. In this scenario, the observer is assumed to have complete (not probe-mediated) access to the target state X, so that the encoding state $\rho(\boldsymbol{v})$ introduced above coincides with the density matrix $\rho_X(\boldsymbol{v})$. In this case, the QFI matrix possesses a simple form in polar coordinates

$$(v_x, v_y, v_z) = (r \sin\theta \cos\phi, r \sin\theta \sin\phi, r \cos\theta), \tag{20}$$

---

[7] Indeed, one can easily verify that the quantity $[(\boldsymbol{H}^{-1})_{jj}]^{-1}$ coincides with the QFI function associated with the estimation of the parameter v_j on the one-parameter family of states $\rho(v_j)$ obtained from $\rho(\boldsymbol{v})$ when assigning fixed values to the other components of $\boldsymbol{v}$.

where it is diagonal. Indeed, using equation (17), one finds

$$\text{Cov}[(r, \theta, \phi)] \geqslant \frac{1}{M} \boldsymbol{H}^{\mathbf{dir}}(r, \theta, \phi)^{-1}, \tag{21}$$

where $\boldsymbol{H}^{\mathbf{dir}}(r, \theta, \phi)$ is the QFI matrix given by

$$\boldsymbol{H}^{\mathbf{dir}}(r, \theta, \phi) = \text{diag}(c_r^{\mathbf{dir}}, c_\theta^{\mathbf{dir}}, c_\theta^{\mathbf{dir}} \sin^2 \theta), \tag{22}$$

with

$$c_r^{\mathbf{dir}} = \frac{1}{1 - r^2}, \qquad c_\theta^{\mathbf{dir}} = r^2. \tag{23}$$

Note that the matrix $\boldsymbol{H}^{\mathbf{dir}}$ does not depend upon the azimuthal angle ϕ while it is a function of the radial coordinate r and on the polar angle θ (the latter however is just a geometric artifact introduced by the polar coordinates: the north and south poles are indeed insensitive to rotations along the *z*-axis).

3. EA strategy

In this section, we will consider the case in which the probe *A* is prepared in an entangled state with the ancilla *B*, i.e. the EA strategy introduced in the previous section and represented in figure 2. More precisely, we will assume that the subsystem *AB* before the scattering is in a maximally entangled state and compute the analytic expression for the associated QFI matrix $\boldsymbol{H}$ as a function of the set of parameters defining the initial state of *X* and of the incident momentum of *A*. In appendix A, we will prove that our results are independent on the specific choice of the maximally entangled input state of *AB*. Henceforth, we will set the input state in the singlet state:

$$\rho_{AB}^{\text{in}} = |\Psi^-\rangle_{AB}\langle\Psi^-|, \quad |\Psi^-\rangle_{AB} = (|0\rangle_A \otimes |1\rangle_B - |1\rangle_A \otimes |0\rangle_B)/\sqrt{2}. \tag{24}$$

3.1. Collecting data in reflection and in transmission

Let us focus first on the experimental setting in which the observer collects both transmitted and reflected signals of the probe *A*.

From expression (17) of the QFI matrix, it immediately follows that the reflection and transmission components of the state $\rho_{AB}^{t+r}(\boldsymbol{v})$ defined in equation (13) provide two separate contributions, as they are associated with orthogonal subspaces. Also, as in the case of the direct estimation discussed in the previous section, it turns out that the QFI matrix possesses a simple form in polar coordinates, where it is diagonal independently of the initial state of *X*. Indeed, upon diagonalization of the state (13), we find that in this case, inequality (21) gets replaced by

$$\text{Cov}[(r, \theta, \phi)] \geqslant \frac{1}{M} \boldsymbol{H}_{\text{EA}}^{t+r}(r, \theta, \phi)^{-1}, \tag{25}$$
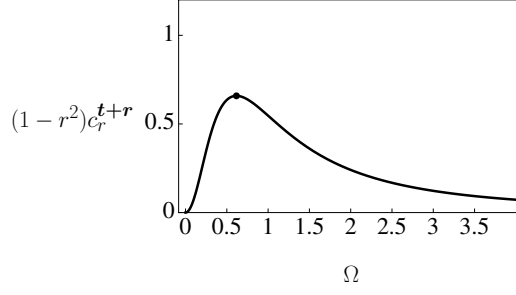
where the QFI matrix is

$$\boldsymbol{H}_{\text{EA}}^{t+r}(r, \theta, \phi) = \text{diag}(c_r^{t+r}, c_\theta^{t+r}, c_\theta^{t+r} \sin^2 \theta), \tag{26}$$

with

$$c_r^{t+r}(r, \Omega) = \frac{8\Omega^2(1 + 18\Omega^2 + 63\Omega^4)}{(1 - r^2)(1 + \Omega^2)(1 + 5\Omega^2)(1 + 9\Omega^2)^2}, \tag{27}$$

Figure 3. Functional dependence of the rescaled QFI function $(1 - r^2)c_r^{t+r}$, whose inverse bounds the accuracy (29) achievable in the determination of r with an EA strategy where AB is initialized in a maximally entangled state and data are collected both in transmission and in reflection cases. The dot indicates the optimal incoming momentum for probe A.

$$
c_\theta^{t+r}(r, \Omega) = \frac{1}{(1+\Omega^2)(1+9\Omega^2)}[4(1+5\Omega^2)(1+9\Omega^2)(1+18\Omega^2+63\Omega^4)
$$
$$
- r^2(1+4\Omega^2+68\Omega^4+720\Omega^6+1863\Omega^8)]
$$
$$
\times \frac{32r^2\Omega^2}{[4(1+9\Omega^2)^2-r^2(1-9\Omega^2)^2][4(1+5\Omega^2)^2-r^2(1+3\Omega^2)^2]} \tag{28}
$$

(in appendix B, we also report the expression of the bound in Cartesian coordinates). As in the case of the direct estimation, H_{EA}^{t+r} does not depend upon the azimuthal angle ϕ, while it is a function of the radial coordinate r and the polar angle θ. Such a behavior is associated with the symmetry of the coupling Hamiltonian (2), which does not possess a preferred spatial direction, and of the input state of AB.[8] It is also worth pointing out that the matrix H_{EA}^{t+r} vanishes when Ω is zero or infinite (i.e. infinite or zero incident momentum $\hbar k$ of the probe A). This implies that for such configurations no recovering of information on X is possible. Indeed if $k = 0$, it means that A is initially at rest and will not be able to be scattered by X, while for very large k it means that A propagates so fast along the line that the interaction with X can only have a minimal (asymptotically vanishing) impact on its evolution.

As a specific example, suppose then that the observer, already knowing the value of the parameters θ and ϕ, is interested in recovering the missing parameter r, which determines the purity of the target system X: $\mathrm{Tr}\,\rho_X^2(\mathbf{v}) = r^2$. Equation (25) then yields

$$
\mathrm{Var}[r] \geqslant \frac{1}{M}\frac{1}{c_r^{t+r}(r,\Omega)} = \frac{1-r^2}{M}\frac{(1+\Omega^2)(1+5\Omega^2)(1+9\Omega^2)^2}{8\Omega^2(1+18\Omega^2+63\Omega^4)}, \tag{29}
$$

which should be compared with the quantity $(1/M)(1/c_r^{\mathbf{dir}}) = (1-r^2)/M$ that one obtains in the direct estimation case, i.e. equations (21)–(23). Since the rational function of Ω on the rhs of equation (29) is larger than 1, it follows that $(1/M)(1/c_r^{\mathbf{dir}})$ is always smaller than the EA bound (this is very much expected since in the case of direct estimation, the observer has access to the X system, while in the EA strategy he/she can only recover info on X through the probe A). The minimum of the rhs of equation (29) is reached when $\Omega \simeq 0.616$ as shown in figure 3; this value provides the optimal input momentum $\hbar k$ of A via equation (6), for recovering the parameter r. For such a choice, the EA strategy misses the direct estimation accuracy just by a factor of 1.52. Note finally that for both the EA strategy and for the direct one, the accuracy bounds vanish with the $\sqrt{1-r^2}$ distance from the surface of the Bloch

---

[8] We stress that the dependence of H_{EA}^{t+r} on θ has nothing to do with the probe–target coupling: as in the case of $H^{\mathbf{dir}}$, it is a geometric artifact of the polar representation.

sphere. (This is a consequence of the fact that it is intrinsically simpler to distinguish pure states from mixed states.)

Consider next the case in which the observer, already knowing the value of the parameters r and θ, is interested in recovering the azimuthal phase ϕ of the target system X. This is given by the third diagonal element of the QFI matrix (26), i.e.

$$\text{Var}[\phi] \geqslant \frac{1}{M} \frac{1}{c_\theta^{t+r}(r, \Omega) \sin^2 \theta}, \tag{30}$$

which again should be compared with the bound $(1/M)(1/c_\theta^{\textbf{dir}} \sin^2 \theta) = (1/M)(1/r^2 \sin^2 \theta)$ one obtains for the direct estimation. Again one can verify that the rhs of equation (30) is always larger than the direct estimation threshold (note however that both expressions diverge for $\theta = 0$ and $\theta = \pi$ due to fact that for such choices the variable ϕ is not even defined). For the sake of simplicity, we focus on the special case in which X is in a pure state on the equatorial plane of the Bloch sphere (i.e. $\theta = \pi/2$ and $r = 1$). In this case, equation (30) yields

$$\text{Var}[\phi] \geqslant \frac{1}{M} \frac{3(1 + \Omega^2)(1 + 3\Omega^2)(1 + 7\Omega^2)(1 + 9\Omega^2)}{32\Omega^2(1 + 10\Omega^2 + 27\Omega^4)}, \tag{31}$$

which reaches its minimum when $\Omega \simeq 0.637$, where the rhs is $\simeq 1.354/M$, falling short of the direct threshold $1/M$ by 35%.

3.2. Collecting only reflected or transmitted data

By repeating the same analysis for the case in which only transmitted or reflected probes are detected (see equations (14) and (15)) we find that equation (25) still holds with the QFI matrix $\boldsymbol{H}_{\text{EA}}^{t+r}(r, \theta, \phi)$ being replaced by

$$\boldsymbol{H}_{\text{EA}}^{t/r}(r, \theta, \phi) = \text{diag}(c_r^{t/r}, c_\theta^{t/r}, c_\theta^{t/r} \sin^2 \theta), \tag{32}$$

with

$$c_r^t(r, \Omega) = \frac{2\Omega^2[3(1 + 3\Omega^2)(11 + 76\Omega^2 + 117\Omega^4) - 2r^2(9 + 50\Omega^2 + 45\Omega^4)]}{(1 - r^2)(1 + \Omega^2)(1 + 5\Omega^2)(1 + 9\Omega^2)[9(1 + 3\Omega^2)^2 - 4r^2]}, \tag{33}$$

$$c_\theta^t(r, \Omega) = \frac{4r^2\Omega^2[2(1 + 5\Omega^2)(11 + 76\Omega^2 + 117\Omega^4) - r^2(1 + 3\Omega^2)^2]}{3(1 + \Omega^2)(1 + 3\Omega^2)(1 + 9\Omega^2)[4(1 + 5\Omega^2)^2 - r^2(1 + 3\Omega^2)^2]}, \tag{34}$$

in transmission, while

$$c_r^r(r, \Omega) = \frac{2\Omega^2[(1 + 7\Omega^2)(1 + 36\Omega^2 + 207\Omega^4) - 2r^2\Omega^2(1 + 18\Omega^2 + 117\Omega^4)]}{(1 - r^2)(1 + \Omega^2)(1 + 9\Omega^2)^2[(1 + 7\Omega^2)^2 - 4r^2\Omega^4]}, \tag{35}$$

$$c_\theta^r(r, \Omega) = \frac{4r^2\Omega^2[2(1 + 9\Omega^2)(1 + 36\Omega^2 + 207\Omega^4) - r^2\Omega^2(1 - 9\Omega^2)^2]}{(1 + \Omega^2)(1 + 7\Omega^2)(1 + 9\Omega^2)[4(1 + 9\Omega^2)^2 - r^2(1 - 9\Omega^2)^2]}, \tag{36}$$

in reflection.

Note that, in this case, even if there is still a quadratic divergence of c_r^r and c_r^t at $r = 1$, their dependence on r does not factorize. Hence, in the estimation of the radius r, the bound (29) is replaced by a lower bound $(1/M)(1/c_r^{t/r})$, which for every value of r admits an optimal momentum for the incident probe A that maximizes the associated QFI, as shown in figures 4 and 5. Interestingly enough, however, there exist 'optimality intervals' for the incident momentum (i.e. $\Omega \in [0.51, 0.55]$ for transmission, and $\Omega \in [0.67, 0.68]$ for reflection), which guarantee rather high performances for all values of r. Observe that in order to achieve the optimal estimation from transmitted data, we have to send the probe faster than the case
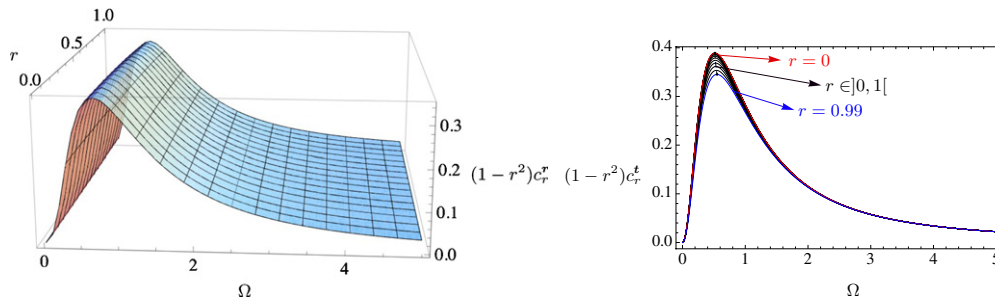
Figure 4. Plots of the rescaled QFI coefficient $(1-r^2)c_r^t(r, \Omega)$ of equation (33) for the transmission case as a function of r and Ω. For every value of r, there exists an optimal value of the incident momentum k. The upper and lower curves in the right panel refer to the case of completely mixed (i.e. $r = 0$) and almost pure states (i.e. $r \simeq 1$), respectively.
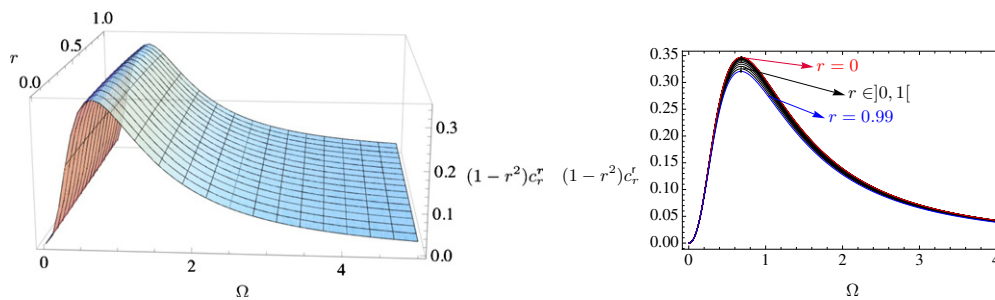
**Figure 5.** As in figure 4, when only reflected data are collected.

of reflection (recall that $\Omega \propto 1/k$): this is in perfect agreement with the intuitive idea that to efficiently collect the data in transmission, A should be given a sufficiently large initial momentum to prevent backscattering from X (and vice versa for reflection). Between the above two intervals lies the optimal value of Ω for the case in which we collect all scattering data, $\Omega \simeq 0.61$.

In figure 6, we plot the QFI of the radius r (purity) for the case of transmitted, reflected, or both reflected and transmitted data. Of course, the last case leads to the best estimation of the target purity, as we are collecting the largest amount of information from the scattering process.

Analogous considerations apply also to the estimation of the polar and azimuthal angles. One can easily extract them by a direct comparison of the coefficients (34) and (36) with the corresponding expression associated with the transmission *and* reflection strategy given in equation (28) and also with the direct estimation procedure [see equation (23)].

4. Comparing EA and NEA strategies

In this section, we will present a comparison between the EA strategies introduced in the previous section with the NEA strategies obtained by restricting the analysis to the case in which the initial state ρ_{AB} of the probe A and the ancilla B is separable. For the sake of simplicity, we find it instructive to restrict the analysis to the situation in which, as in figure 6, the observer aims only to estimate the purity of the target state X. Specifically, we will work

11
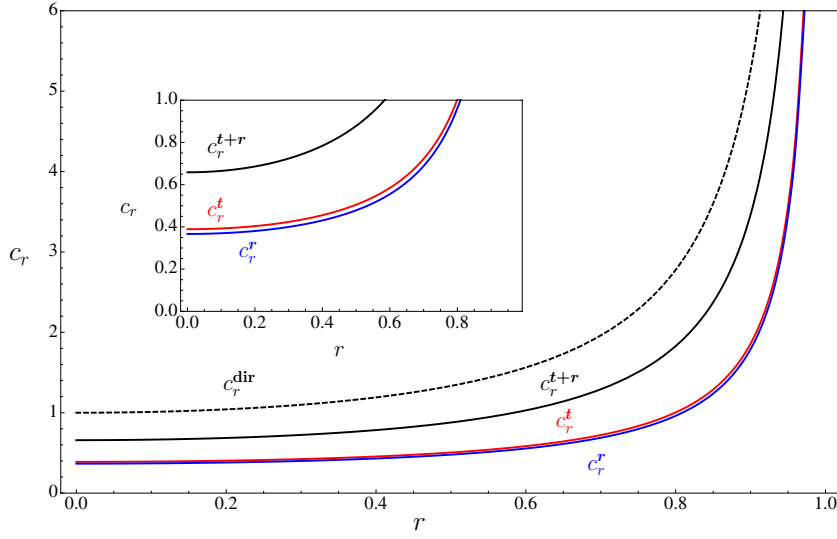
Figure 6. Plot of the quantum CR bound for rescaled variance $M \text{Var}[r]$, of the estimation of the radius r of the Bloch sphere describing the target qubit, in polar coordinates. The dashed line denotes the ultimate limit achievable by direct access to the target, while the solid lines denote the case in which both reflected and transmitted, only transmitted and only reflected data are collected. In particular, the case of both reflected and transmitted data is plotted at the optimal value $\Omega \simeq 0.61$, which, in this case, is independent of the value of r. The case in which only reflected or only transmitted data are collected has been plotted instead by considering, for each given r, the corresponding optimal value of Ω. Note that for all values of r, we find $c_r^{t+r} > c_r^{t/r}$, since by collecting all the scattering data, we gain the largest amount of information on the target. Furthermore, observe that transmission and reflection give almost the same result, with a little improvement of transmission with respect to reflection.

under the assumption that the three-dimensional vector $\boldsymbol{v}$ that specifies $\rho_X(\boldsymbol{v})$ in the Bloch sphere lies on the z-axis, i.e. $v_x = v_y = 0$ and

$$\rho_X(v_z) = \frac{1 + v_z \sigma_X^z}{2}, \qquad v_z \in [-1, 1]. \tag{37}$$

Under this condition, the quantum CR bound (16) reduces to an inequality for the variance $\text{Var}[v_z]$ of the unique parameter v_z, i.e.

$$\text{Var}[v_z] \geqslant \frac{1}{M} H_{\text{EA/NEA}}^{t+r/t/r}(v_z)^{-1}, \tag{38}$$

where $H_{\text{EA/NEA}}^{t+r/t/r}(v_z)$ are the QFI functions of the problem computed as usual by exploiting the spectral decomposition of the output states AB/A and using equation (17) (which in this case contains only derivatives with respect of the unique parameter v_z).

For the EA configuration, the functions $H_{\text{EA}}^{t+r/t/r}(v_z)$ coincide with the third diagonal elements of the QFI matrices in Cartesian coordinates evaluated at $v_x = v_y = 0$, namely

$$H_{\text{EA}}^{t+r}(v_z) = \frac{8\Omega^2(1 + 18\Omega^2 + 63\Omega^4)}{(1 - v_z^2)(1 + \Omega^2)(1 + 5\Omega^2)(1 + 9\Omega^2)^2}, \tag{39}$$

$$H_{\text{EA}}^{t}(v_z) = \frac{2\Omega^2[3(1 + 3\Omega^2)(11 + 76\Omega^2 + 117\Omega^4) - 2v_z^2(9 + 50\Omega^2 + 45\Omega^4)]}{(1 - v_z^2)(1 + \Omega^2)(1 + 5\Omega^2)(1 + 9\Omega^2)[9(1 + 3\Omega^2)^2 - 4v_z^2]}, \tag{40}$$

$$H_{\text{EA}}^{r}(v_z) = \frac{2\Omega^2[(1+7\Omega^2)(1+36\Omega^2+207\Omega^4) - 2v_z^2\Omega^2(1+18\Omega^2+117\Omega^4)]}{(1-v_z^2)(1+\Omega^2)(1+9\Omega^2)^2[(1+7\Omega^2)^2 - 4v_z^2\Omega^4]}. \tag{41}$$

Note that the above expressions can be retrieved from equations (27), (33) and (35) by substituting r with v_z. The general expression of the QFI matrix for the EA configuration can be found in appendix B.

Before computing the QFI functions for the NEA configuration, it is worth observing that due to the convexity of the QFI function (e.g. see [16]), it follows that in the NEA scenario the contribution of the ancilla B in the scattering can be completely neglected, see figure 2. Indeed, since the maximum of a QFI function is always achieved on pure states, one can restrict the analysis of the NEA configuration to pure separable states of AB: for them however the output states of AB also factorize and one can completely ignore the subsystem B. Consequently, the states of the system after the scattering are given by equations (9), (10) or (12), for the case in which we collect either all scattering data, or only transmitted/reflected probes. In particular, we will assume

$$\rho_A^{\text{in}} = \frac{1 + \boldsymbol{n} \cdot \boldsymbol{\sigma}_A}{2}, \qquad \boldsymbol{n} = (\sin\theta_A, 0, \cos\theta_A), \tag{42}$$

where, without loss of generality, the input azimuthal angle ϕ_A has been set to zero by using the symmetry of the coupling Hamiltonian.

Let us then consider first the accuracy achievable when collecting data only on transmission, i.e. assuming as an output state the one given in equation (10). The resulting QFI is the following (involved) function of θ_A:

$$\begin{aligned}
H_{\text{NEA}}^{t}(v_z, \theta_A, \Omega) = {} & [4(11+96\Omega^2+181\Omega^4) - v_z^2(1+\Omega^2)(1+33\Omega^2) \\
& - 4v_z(8+43\Omega^2+3\Omega^4)\cos\theta_A - 4(1-\Omega^2+8v_z^2\Omega^2)(1+\Omega^2)\cos 2\theta_A \\
& - 4v_z\Omega^2(1+\Omega^2)\cos 3\theta_A + v_z^2(1+\Omega^2)^2\cos 4\theta_A] \\
& \times \frac{1}{4(1+5\Omega^2) - v_z^2(1+17\Omega^2) - v_z(1+\Omega^2)(4\cos\theta_A - v_z\cos 2\theta_A)} \\
& \times \frac{\Omega^2}{(1+\Omega^2)(3+9\Omega^2-2v_z\cos\theta_A)(1+7\Omega^2+2v_z\Omega^2\cos\theta_A)}.
\end{aligned} \tag{43}$$

Still one recognizes some general features that we already observed in the previous section. In particular, the QFI function vanishes at $\Omega = 0$ and $\Omega = \infty$. Note also that when the target state is pure, there exists a particular choice of the initial state of the probe such that the above quantity diverges quadratically, as found for the EA strategy, namely $v_z = 1$, $\theta_A = 0$ and $v_z = -1$, $\theta_A = \pi$, and arbitrary (finite) $\Omega > 0$. Finally, note that for each value of v_z, there exists an optimal point for the pair (θ_A, Ω) that maximizes the QFI. In figure 7, we plot the envelope of the QFI for $v_z \in [-1, 1]$ that is the maximum value of $H_{\text{NEA}}^{t}(v_z)$, which can be proved to be a symmetric function of v_z. Note that the initial state of A that yields the best estimation of the target state depends on v_z, i.e. on the initial state of the target, which is in principle unknown. We can only say that once we have set the direction of the probe A in the Bloch sphere before the scattering, the best optimization we can obtain involves pure target states with Bloch vectors parallel to this direction. The same analysis can be repeated for reflection and yields

$$\begin{aligned}
H_{\text{NEA}}^{r}(v_z, \theta_A, \Omega) = {} & [4(5+23\Omega^2) - v_z^2(1+\Omega^2) - 4v_z(3-2\Omega^2)\cos\theta_A \\
& + 4(1-5\Omega^2)\cos 2\theta_A - 4v_z(1+2\Omega^2)\cos 3\theta_A + v_z^2(1+\Omega^2)\cos 4\theta_A]
\end{aligned}$$
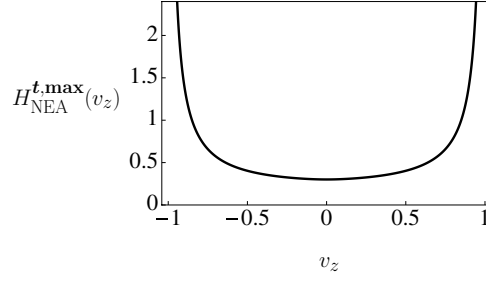
Figure 7. Envelope of the QFI for the NEA configuration corresponding to the optimal choice of θ_A and Ω for each value of v_z, if only transmitted data are collected. Note the divergence at $v_z = \pm 1$, which for all Ω corresponds to $\theta_A = 0$ and π.

$$\times \frac{1}{3(1 + 3\Omega^2)(1 + 7\Omega^2) - 2v_z^2\Omega^2 - 2v_z(1 + 4\Omega^2 - 9\Omega^4)\cos\theta_A - 2v_z^2\Omega^2\cos 2\theta_A}$$

$$\times \frac{\Omega^2}{(1 + \Omega^2)(4 - v_z^2 - 4v_z\cos\theta_A + v_z^2\cos 2\theta_A)}. \tag{44}$$

Similarly to the case of transmission, the optimal values of θ_A and Ω are symmetric functions of v_z. Moreover, when the target state is pure, i.e. $v_z = 1$ and -1, the QFI diverges for $\theta_A = 0$ and π, respectively, as for transmission.

Finally, the largest amount of information on the system can be inferred by collecting both transmitted and reflected data. In this case, the QFI associated with the state (9) of the incident probe after the scattering is given by

$$
\begin{aligned}
H_{\text{NEA}}^{t+r}(v_z, \theta_A, \Omega) = \{&(1 + 7\Omega^2 + 2v_z\Omega^2\cos\theta_A) \\
&\times [4(1 + 5\Omega^2) - v_z^2(1 + 17\Omega^2) - v_z(1 + \Omega^2)(4\cos\theta_A - v_z\cos 2\theta_A)] \\
&\times [4(5 + 27\Omega^2) - v_z^2 + 4(1 - 9\Omega^2)\cos 2\theta_A - 16v_z\cos\theta_A^3 + v_z^2\cos 4\theta_A] \\
&+ (4 - v_z^2 - 4v_z\cos\theta_A + v_z^2\cos 2\theta_A)[3(1 + 3\Omega^2) - 2v_z\cos\theta_A] \\
&\times [4(3 + 48\Omega^2 + 181\Omega^4) - v_z^2\Omega^2(1 + 33\Omega^2) - 12v_z\Omega^2(1 + \Omega^2)\cos\theta_A \\
&- 4(1 + 8\Omega^2 - \Omega^4 + 8v_z^2\Omega^4)\cos 2\theta_A - v_z\Omega^2(1 + \Omega^2)(4\cos 3\theta_A - v_z\cos 4\theta_A)]\} \\
&\times \frac{1}{4(1 + 5\Omega^2) - v_z^2(1 + 17\Omega^2) - v_z(1 + \Omega^2)(4\cos\theta_A - v_z\cos 2\theta_A)} \\
&\times \frac{1}{(4 - v_z^2 - 4v_z\cos\theta_A + v_z^2\cos 2\theta_A)(3 + 9\Omega^2 - 2v_z\cos\theta_A)} \\
&\times \frac{\Omega^2}{(1 + \Omega^2)(1 + 9\Omega^2)(1 + 7\Omega^2 + 2v_z\Omega^2\cos\theta_A)}. \tag{45}
\end{aligned}
$$

This function exhibits the same properties as H_{NEA}^t and H_{NEA}^r. The three curves plotted in figure 8, all symmetric with respect to v_z, refer to the optimal values of the QFI for the three cases analyzed above. As expected, the collection of all scattering data returns the best tomographic reconstruction of the target state. Note that the transmission strategy seems to overcome the reflection one, like in the EA strategy. Also, it can be shown that for all v_z, the optimal value of Ω for the transmission is lower than that for reflection, and for the case in which we collect both transmitted and reflected data, it is in-between (these results have been obtained by numerical optimizations).

In order to compare the efficiency of the NEA strategies with the EA strategies discussed in the previous section, in figure 9, we plot the maximum QFI for $v_z \geqslant 0$, for the EA (solid line) and the NEA (dashed line) strategies (the expression for the EA strategies have been
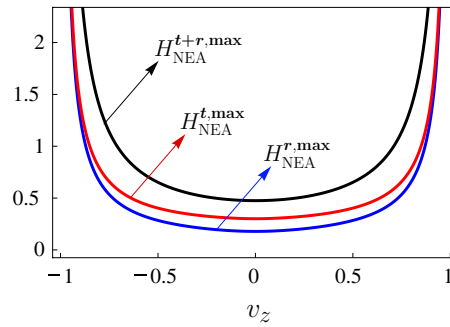
Figure 8. Envelope of the QFI for the NEA strategy corresponding to the optimal choice of θ_A and Ω for each value of v_z, for the case in which we collect either transmitted, or reflected or all scattered probes. Note that the QFI diverges for $v_z = 1$ and -1 when $\theta_A = 0$ and π, respectively.
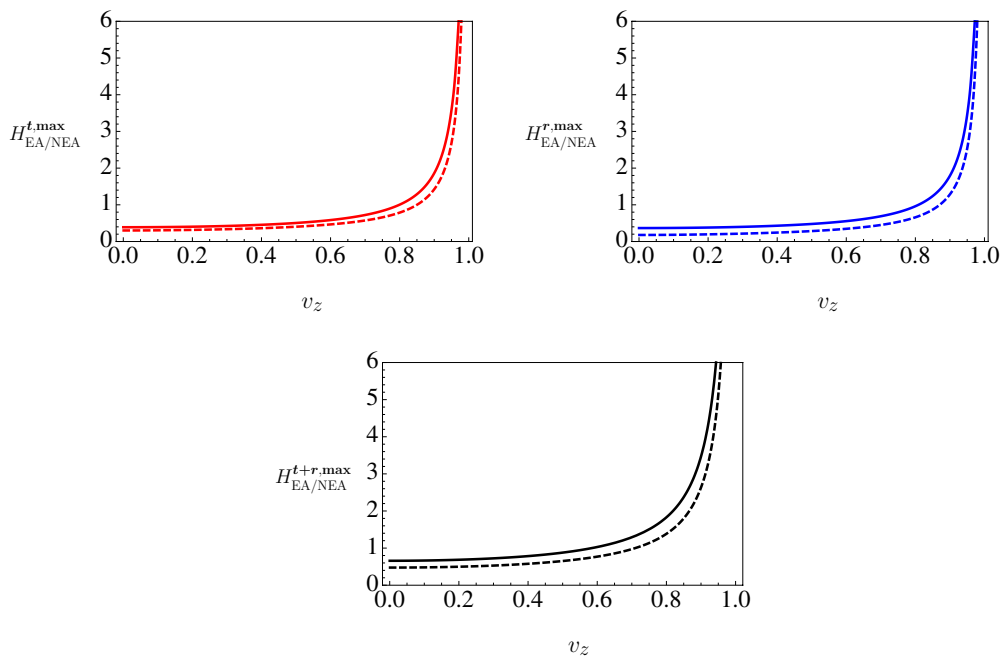
Figure 9. The maximum value of the QFI associated with the parameter v_z of the target qubit X. The solid line denotes the EA strategy, where the probe A is in a maximally entangled state with the ancilla B, while the dashed line denotes the NEA.

obtained by exploiting the representation of the QFI matrix in Cartesian coordinates reported in appendix B). The role played by the entanglement between the probe and the ancilla before the scattering is evident: it implies an enhancement in the QFI for all v_z, both for the case in which we collect all the scattering data and for the case in which we have access only to transmission/reflection events.

5. Conclusion

We have presented a detailed study of the tomographic state reconstruction of a target system, obtained by monitoring a scattered probe. Focusing on the special case in which both the

15

target and the probe are qubit systems, and assuming the scattering to take place on a 1D line, we used quantum estimation techniques to evaluate the efficiency of the process in several configurations of interest. In particular, we distinguished two regimes: the EA regime in which the observer is allowed to initialize the probe in an entangled state with an external ancilla that it is kept in the laboratory, and the NEA regime where instead no entanglement is allowed between the probe and the ancilla. As expected, when all the other settings are kept identical, the EA strategies turn out to be more effective then their NEA counterparts.

Within both regimes, we have also studied what happens when the observers have access to all or only part of the scattered data. Specifically, we consider the cases in which only transmitted or reflected data are used in the tomographic reconstruction, noting that these regimes are characterized by different optimal values for the input momentum of the probing particle (the transmitted scenario being characterized by higher optimal input momenta than the reflected one). We have also analyzed the situation in which both transmitted and reflected data are available to the observer, assuming though that no joint coherent measurements could be performed on the associated quantum degree of freedom (i.e. we explicitly excluded the possibility of performing joint detection on the left and right sides of the 1D channel, an hypothesis which is very much reasonable if the detectors are located at sufficient large distances from each other). The overall accuracy clearly benefits from this possibility: still it remains below the threshold [3] that one obtains when direct access to the target system is allowed. An open problem is to the determine whether or not one could exploit other sort of quantum resources to close such gap. A possible condition that we aim to explore in a future development of the work is to allow the observer to *entangle* different probes together (in the present scenario indeed, even though we used *M* probes, they were all prepared in a factorized configuration of the *same* initial state). This strategy could in fact benefit from super-additivity effects arising from the presence of non-classical correlations between the various probes, resulting in higher performances of the tomographic reconstruction. An interesting open problem is also to understand to what extent the specific features we have observed in our simple scattering model (qubits interacting along a 1D line via the Heisenberg-like coupling) could be generalize to more complex configurations (say by increasing the size of the target and/or of the probe, or by allowing the scattering to take place in a 2D or a 3D setting).

Acknowledgments

Appendix A. Equivalence between maximally entangled states

We explicitly prove that our analysis for the EA strategies is independent of the particular choice of a maximally entangled state for the subsystem *AB*.

The Heisenberg-type coupling $\boldsymbol{\sigma}_X \cdot \boldsymbol{\sigma}_A$ describing the interaction between qubits *X* and *A* can be written in terms of the so-called *swap operator* $\mathcal{S}_{X|A}$ as

$$\boldsymbol{\sigma}_X \cdot \boldsymbol{\sigma}_A = 2\mathcal{S}_{X|A} - \mathbb{I}_{XA}, \qquad \mathcal{S}_{X|A} = \sum_{i,j} |i\rangle_X \langle j| \otimes |j\rangle_A \langle i|. \tag{A.1}$$

It is a unitary self-adjoint operator and is characterized by the following very simple property:

$$(\mathbb{I}_X \otimes U_A)\mathcal{S}_{X|A}(\mathbb{I}_X \otimes U_A^\dagger) = (U_X^\dagger \otimes \mathbb{I}_A)\mathcal{S}'_{X|A}(U_X \otimes \mathbb{I}_A), \tag{A.2}$$

where U_X and U_A act in the same way on $\mathcal{H}_X$ and $\mathcal{H}_A$, respectively ($U_X = U_A$), and $\mathcal{S}'_{X|A}$ is the swap operator in the rotated frame

$$\mathcal{S}'_{X|A} = \sum_{i,j} |r_i\rangle_X \langle r_j| \otimes |r_j\rangle_A \langle r_i|, \qquad |r_i\rangle_{X/A} = U_{X/A}|i\rangle_{X/A}. \tag{A.3}$$

The above property is trivially conserved for the interaction Hamiltonian $\boldsymbol{\sigma}_X \cdot \boldsymbol{\sigma}_A$. The equivalence among all the maximally entangled input states for the EA strategies is thus straightforward. Indeed, a generic maximally entangled state of the probe A and the ancilla B can always be written as $|\Psi_{UV}\rangle_{AB} = (U_A^\dagger \otimes V_B^\dagger)|\Psi^-\rangle_{AB}$, with $|\Psi^-\rangle_{AB}$ being the singlet state (24). If we send $|\Psi_{UV}\rangle_{AB}$ to the target qubit X, it can be easily shown that the contributions given by $\mathrm{Tr}_X\{\ldots\}$ in the final state of the subsystem AB become

$$(U_A^\dagger \otimes V_B^\dagger)\,\mathrm{Tr}_X[(U_A S_{XA}^{t/r} U_A^\dagger)(\rho_X(\boldsymbol{v}) \otimes |\Psi^-\rangle_{AB}\langle\Psi^-|)(U_A S_{XA}^{t/r\,\dagger} U_A^\dagger)](U_A \otimes V_B)$$
$$= (U_A^\dagger \otimes V_B^\dagger)\,\mathrm{Tr}_X[S_{XA}'^{t/r}(\rho_X'(\boldsymbol{v}) \otimes |\Psi^-\rangle_{AB}\langle\Psi^-|)S_{XA}'^{t/r\,\dagger}](U_A \otimes V_B) \tag{A.4}$$

with

$$S_{XA}'^{t,r} = \alpha_{t,r}(\Omega) + \beta_{t,r}(\Omega)(2\mathcal{S}'_{X|A} - \mathbb{I}_{XA}), \qquad \rho_X' = U_X \rho_X U_X^\dagger. \tag{A.5}$$

Since the physical properties of the system do not depend on the choice of the reference basis, the results of our analysis for the EA strategies are completely independent of the choice of an initial maximally entangled state of AB.

Appendix B. QFI matrix in Cartesian coordinates

In this appendix, we consider the explicit expression of the Fisher matrix for the EA strategy and discuss the symmetry properties of its elements.

For the case in which both transmitted and reflected probes are collected, the off-diagonal elements of the Fisher matrix are given by

$$[\boldsymbol{H}_{\mathrm{EA}}^{t+r}(v_x, v_y, v_z)]_{ij,i\neq j} = \frac{2v_i v_j \Omega^2}{(1 - \boldsymbol{v}^2)(1 + \Omega^2)(1 + 5\Omega^2)(1 + 9\Omega^2)^2}$$
$$\times \{(1 + 7\Omega^2)(1 + 9\Omega^2)(3 + 13\Omega^2)^2[4(1 + 9\Omega^2)^2 - \boldsymbol{v}^2(1 - 9\Omega^2)^2]$$
$$+ 3(1 + 3\Omega^2)(1 + 5\Omega^2)(1 + 27\Omega^2)^2[4(1 + 5\Omega^2)^2 - \boldsymbol{v}^2(1 + 3\Omega^2)^2]\}$$
$$\times \frac{1}{[4(1 + 9\Omega^2)^2 - \boldsymbol{v}^2(1 - 9\Omega^2)^2][4(1 + 5\Omega^2)^2 - \boldsymbol{v}^2(1 + 3\Omega^2)^2]}, \tag{B.1}$$

with $i, j \in \{x, y, z\}$, while for the diagonal elements, we have

$$[\boldsymbol{H}_{\mathrm{EA}}^{t+r}(v_x, v_y, v_z)]_{ii} = \frac{2\Omega^2}{(1 - \boldsymbol{v}^2)(1 + \Omega^2)(1 + 5\Omega^2)(1 + 9\Omega^2)^2}$$
$$\times \{(1 + 9\Omega^2)(3 + 13\Omega^2)[4(1 + 9\Omega^2)^2 - \boldsymbol{v}^2(1 - 9\Omega^2)^2]$$
$$\times [v_i^2(1 + 7\Omega^2)(3 + 13\Omega^2) + 4(1 - \boldsymbol{v}^2)(1 + 5\Omega^2)^2]$$
$$+ (1 + 5\Omega^2)(1 + 27\Omega^2)[4(1 + 5\Omega^2)^2 - \boldsymbol{v}^2(1 + 3\Omega^2)^2]$$
$$\times [3v_i^2(1 + 3\Omega^2)(1 + 27\Omega^2) + 4(1 - \boldsymbol{v}^2)(1 + 9\Omega^2)^2]\}$$
$$\times \frac{1}{[4(1 + 9\Omega^2)^2 - \boldsymbol{v}^2(1 - 9\Omega^2)^2][4(1 + 5\Omega^2)^2 - \boldsymbol{v}^2(1 + 3\Omega^2)^2]}, \tag{B.2}$$

with $i, j \in \{x, y, z\}$. Note that if there is only one out of the three parameters characterizing the initial state of the target different from zero, $v_i \neq 0$ and $v_j = v_k = 0$, the QFI matrix is

diagonal and thus its *ii* element coincides with the single-parameter QFI for v_i. Furthermore, due to the symmetry of the Heisenberg-type interaction and of the singlet state of *A* and *B* before the scattering, we find

$$(1 - v_i{}^2)[\boldsymbol{H}_{\text{EA}}^{t+r}(v_x, v_y, v_z)]_{ii} = (1 - r^2)c_r^{t+r}, \qquad i \in \{x, y, z\}. \tag{B.3}$$

If we are able to detect only transmitted or reflected probes, we obtain

$$
\begin{aligned}
{}[\boldsymbol{H}_{\text{EA}}^{t}(v_x, v_y, v_z)]_{ij,i\neq j} =\ & \frac{2v_i v_j \Omega^2}{3(1 - \boldsymbol{v}^2)(1 + \Omega^2)(1 + 3\Omega^2)(1 + 5\Omega^2)(1 + 9\Omega^2)} \\
& \times \{[3(1 + 3\Omega^2)(1 + 7\Omega^2)(3 + 13\Omega^2)^2[9(1 + 3\Omega^2)^2 - 4\boldsymbol{v}^2] \\
& + 8(1 - \boldsymbol{v}^2)(1 + 5\Omega^2)[4(1 + 5\Omega^2)^2 - \boldsymbol{v}^2(1 + 3\Omega^2)^2]\} \\
& \times \frac{1}{[9(1 + 3\Omega^2)^2 - 4\boldsymbol{v}^2][4(1 + 5\Omega^2)^2 - \boldsymbol{v}^2(1 + 3\Omega^2)^2]},
\end{aligned}
\tag{B.4}
$$

$$
\begin{aligned}
{}[\boldsymbol{H}_{\text{EA}}^{t}(v_x, v_y, v_z)]_{ii} =\ & \frac{2\Omega^2}{3(1 - \boldsymbol{v}^2)(1 + \Omega^2)(1 + 3\Omega^2)(1 + 5\Omega^2)(1 + 9\Omega^2)} \\
& \times \{2(1 - \boldsymbol{v}^2)(1 + 5\Omega^2)[4(1 + 5\Omega^2)^2 - \boldsymbol{v}^2(1 + 3\Omega^2)^2] \\
& \times [9(1 + 3\Omega^2)^2 - 4(v_j^2 + v_k^2)] \\
& + 3(1 + 3\Omega^2)(3 + 13\Omega^2)[9(1 + 3\Omega^2)^2 - 4\boldsymbol{v}^2] \\
& \times [4(1 + 5\Omega^2)^2(1 - v_j^2 - v_k^2) - (1 + 3\Omega^2)^2 v_i^2]\} \\
& \times \frac{1}{[9(1 + 3\Omega^2)^2 - 4\boldsymbol{v}^2][4(1 + 5\Omega^2)^2 - \boldsymbol{v}^2(1 + 3\Omega^2)^2]},
\end{aligned}
\tag{B.5}
$$

and

$$
\begin{aligned}
{}[\boldsymbol{H}_{\text{EA}}^{r}(v_x, v_y, v_z)]_{ij,i\neq j} =\ & \frac{2v_i v_j \Omega^2}{(1 - \boldsymbol{v}^2)(1 + \Omega^2)(1 + 7\Omega^2)(1 + 9\Omega^2)^2} \\
& \times \{3(1 + 3\Omega^2)(1 + 7\Omega^2)(1 + 27\Omega^2)^2[(1 + 7\Omega^2)^2 - 4\boldsymbol{v}^2\Omega^4] \\
& - 8(1 - \boldsymbol{v}^2)\Omega^6(1 + 9\Omega^2)[4(1 + 9\Omega^2)^2 - \boldsymbol{v}^2(1 - 9\Omega^2)^2]\} \\
& \times \frac{1}{[(1 + 7\Omega^2)^2 - 4\boldsymbol{v}^2\Omega^4][4(1 + 9\Omega^2)^2 - \boldsymbol{v}^2(1 - 9\Omega^2)^2]},
\end{aligned}
\tag{B.6}
$$

$$
\begin{aligned}
{}[\boldsymbol{H}_{\text{EA}}^{r}(v_x, v_y, v_z)]_{ii} =\ & \frac{2\Omega^2}{(1 - \boldsymbol{v}^2)(1 + \Omega^2)(1 + 7\Omega^2)(1 + 9\Omega^2)^2} \\
& \times \{(1 + 7\Omega^2)(1 + 27\Omega^2)[(1 + 7\Omega^2)^2 - 4\boldsymbol{v}^2\Omega^4] \\
& \times [4(1 + 9\Omega^2)^2(1 - v_j^2 - v_k^2) - v_i^2(1 - 9\Omega^2)^2] \\
& + 2(1 - \boldsymbol{v}^2)\Omega^2(1 + 9\Omega^2)[4(1 + 9\Omega^2)^2 - \boldsymbol{v}^2(1 - 9\Omega^2)^2] \\
& \times ((1 + 7\Omega^2)^2 - 4\Omega^4(v_j^2 - v_k^2))\} \\
& \times \frac{1}{[(1 + 7\Omega^2)^2 - 4\boldsymbol{v}^2\Omega^4][4(1 + 9\Omega^2)^2 - \boldsymbol{v}^2(1 - 9\Omega^2)^2]},
\end{aligned}
\tag{B.7}
$$

$\forall i, j, k \in \{x, y, z\}$. Analogously to the case in which we detect all the scattered probes, we find that also for the transmission and the reflection cases if we have $v_i \neq 0$ and $v_j = v_k = 0$, $i \neq j \neq k \in \{x, y, z\}$, the QFI for v_i is diagonal, and furthermore, an equation similar to (B.3) holds:

$$(1 - v_i{}^2)[\boldsymbol{H}_{\text{EA}}^{t/r}(v_x, v_y, v_z)]_{ii} = (1 - r^2)c_r^{t/r}, \qquad i \in \{x, y, z\}. \tag{B.8}$$

References

[1] Paris M G A and Řeháček J (ed) 2004 *Quantum State Estimation* (Berlin: Springer)
[2] Peres A and Wootters W K 1991 *Phys. Rev. Lett.* **66** 1119
    Jones K R 1994 *Phys. Rev. A* **50** 3682
    Massar S and Popescu S 1995 *Phys. Rev. Lett.* **74** 1259
    Brodyand D and Meister B 1996 *Phys. Rev. Lett.* **76** 1
    Gill R D and Massar S 2000 *Phys. Rev. A* **61** 042312
    Hradil Z, Summhammer J, Badurek G and Rauch H 2000 *Phys. Rev. A* **62** 014101
    Bagan E, Baig M, Brey A, Muñoz-Tapia R and Tarrach R 2000 *Phys. Rev. Lett.* **85** 5230
    Massar S 2001 *Phys. Rev. A* **62** 040101
    Bagan E, Baig M, Brey A, Muñoz-Tapia R and Tarrach R 2001 *Phys. Rev. A* **63** 052309
    Peres A and Scudo P F 2001 *Phys. Rev. Lett.* **86** 4160
    Bagan E, Baig M and Muñoz-Tapia R 2001 *Phys. Rev. A* **64** 022305
    Banaszek K and Devetak I 2001 *Phys. Rev. A* **64** 052307
    Matsumoto K 2002 *J. Phys. A: Math. Gen.* **35** 3111
    Hannemann Th, Reiss D, Balzer Ch, Neuhauser W, Toschek P E and Wunderlich Ch 2002 *Phys. Rev. A* **65** 050303
    Bagan E, Baig M and Muñoz-Tapia R 2002 *Phys. Rev. Lett.* **89** 277904
    Embacher F and Narnhofer H 2004 *Ann. Phys.* **311** 220
    Bagan E, Monras A and Muñoz-Tapia R 2005 *Phys. Rev. A* **71** 062318
[3] Bagan E, Ballester M A, Gill R D, Monras A and Muñoz-Tapia R 2006 *Phys. Rev. A* **73** 032301
[4] Helstrom C W 1976 *Quantum Detection and Estimation Theory* (New York: Academic)
[5] Holevo A S 2011 *Probabilistic and Statistical Aspects of Quantum Theory* 2nd edn (Pisa: Edizioni della Normale)
[6] Nielsen M A and Chuang I L 1997 *Phys. Rev. Lett.* **79** 321
[7] Vidal G, Masanes L and Cirac J I 2002 *Phys. Rev. Lett.* **88** 047905
[8] Micŭda M, Ježek M, Dušek M and Fiurášek J 2008 *Phys. Rev. A* **78** 062311
[9] Paris M G A 2009 *Int. J. Quantum Inf.* **7** 125
[10] Giovannetti V, Lloyd S and Maccone L 2011 *Nature Photon.* **5** 222
[11] De Pasquale A, Yuasa K and Nakazato H 2009 *Phys. Rev. A* **80** 052111
[12] Ciccarello F, Palma G M, Zarcone M, Omar Y and Vieira V R 2006 *New J. Phys.* **8** 214
    Ciccarello F, Paternostro M, Kim M S and Palma G M 2008 *Phys. Rev. Lett.* **100** 150501
    Ciccarello F, Paternostro M, Palma G M and Zarcone M 2009 *New J. Phys.* **11** 113053
    Ciccarello F, Paternostro M, Bose S, Browne D E, Palma G M and Zarcone M 2009 *Phys. Rev. A* **82** 030302
    Cordourier-Maruri G, Ciccarello F, Omar Y, Zarcone M, de Coss R and Bose S 2010 *Phys. Rev. A* **82** 052313
[13] Yuasa K and Nakazato H 2007 *J. Phys. A: Math. Theor.* **40** 297
    Yuasa K, Burgarth D, Giovannetti V and Nakazato H 2009 *New J. Phys.* **11** 123027
    Yuasa K 2010 *J. Phys. A: Math. Theor.* **43** 095304
[14] Giovannetti V, Lloyd S and Maccone L 2006 *Phys. Rev. Lett.* **96** 010401
[15] Ji Z, Wang G, Duan R, Feng Y and Ying M 2008 *IEEE Trans. Inf. Theory* **54** 5172
[16] Fujiwara A 2001 *Phys. Rev. A* **63** 042304
    Fisher D G, Mack H, Cirone M A and Freyberger M 2001 *Phys. Rev. A* **64** 022309
    Sasaki M, Ban M and Barnett S M 2002 *Phys. Rev. A* **66** 022308
    Fujiwara A and Imai H 2003 *J. Phys. A: Math. Gen.* **36** 8093
    Ballester M 2004 *Phys. Rev. A* **69** 022303
[17] Costa A T Jr, Bose S and Omar Y 2006 *Phys. Rev. Lett.* **96** 230501
[18] Datta S 1997 *Electronic Transport in Mesoscopic Systems* (Cambridge: Cambridge University Press)
    Harrison P 2005 *Quantum Wells, Wires and Dots* 2nd edn (West Sussex: Wiley)
    Gunlycke D, Jefferson J H, Rejec T, Ramšak A, Pettifor D G and Briggs G A D 2006 *J. Phys.: Condens. Matter* **18** S851
[19] Tans S J, Devoret M H, Dai H, Thess A, Smalley R E, Geerligs L J and Dekker C 1997 *Nature* **386** 474
[20] Kawabata S 2001 *J. Phys. Soc. Japan* **70** 1210
[21] Hayashi T, Fujisawa T, Cheong H D, Jeong Y H and Hirayama Y 2003 *Phys. Rev. Lett.* **91** 226804
    Gorman J, Hasko D G and Williams D A 2005 *Phys. Rev. Lett.* **95** 090502
[22] Cramér H 1946 *Mathematical Methods of Statistics* (Cambridge: Princeton University Press)
[23] Sacchi M F 2005 *Phys. Rev. A* **71** 062340
    Sacchi M F 2005 *Phys. Rev. A* **72** 014305
    Tan S-H, Erkmen B I, Giovannetti V, Guha S, Lloyd S, Maccone L, Pirandola S and Shapiro J H 2008 *Phys. Rev. Lett.* **101** 253601